Case Reviews on the Effect of Microstructure on the Corrosion Behavior of Austenitic Alloys for Processing and Storage of Nuclear Waste

V. KAIN, P. SENGUPTA, P.K. DE, and S. BANERJEE

This article describes the corrosion behavior of special austenitic alloys for waste management applications. The special stainless steels have controlled levels of alloying and impurity elements and inclusion levels. It is shown that "active" inclusions and segregation of chromium along flow lines accelerated IGC of nonsensitized stainless steels. Concentration of Cr^{+6} ions in the grooves of dissolved inclusions increased the potential to the transpassive region of the material, leading to accelerated attack. It is shown that a combination of cold working and controlled solution annealing resulted in a microstructure that resisted corrosion even after a sensitization heat treatment. This imparted extra resistance to corrosion by increasing the fraction of "random" grain boundaries above a threshold value. Randomization of grain boundaries made the stainless steels resistant to sensitization, IGC, and intergranular stress corrosion cracking (IGSCC) in even hot chloride environments. The increased corrosion resistance has been attributed to connectivity of random grain boundaries. The reaction mechanism between the molten glass and the material for process pot, alloy 690, during the vitrification process has been shown to result in depletion of chromium from the reacting surfaces. A comparison is drawn between the electrochemical behavior of alloys 33 and 22 in 1 M HCl at 65 °C. It is shown that a secondary phase formed during welding of alloy 33 impaired corrosion properties in the HCl environment.

I. INTRODUCTION

THE Indian nuclear energy program is envisaged as a three-stage, closed-end fuel cycle program.[1] The first stage is primarily based on natural uranium fueled pressurized heavy water reactors (PWHRs). India has 12 operating PHWRs and 6 are under construction. Two boiling water reactors have been operating since the early 1970s. The Pu^{239} generated from U^{238} is separated by reprocessing and is planned to be used with depleted uranium as fuel in the fast breeder reactors in the second stage. India already operates a 40 MWth fast breeder test reactor and is working on construction of a 500 MWe prototype fast breeder reactor. The third stage of the Indian nuclear program envisages use of our vast thorium resources. This three-stage program has a vast potential for electricity generation for several centuries. The main feature of the Indian nuclear power program thus is the closed-end fuel cycle in which spent fuel from one type of reactors is used for production of fuel for the next generation of reactors. The closed fuel cycle also allows nuclear incineration of long lived fissile isotopes. In India, the reprocessed liquid waste has been stored in metallic tanks. The vitrification plant[2] commissioned in 2002 is used to minimize the problem of large volumes of waste to be stored for a long term. This calls for materials and corrosion control strategies to have a safe and trouble-free operation of the waste management plants.

Storage of liquid nuclear waste requires that the metallic tanks have excellent corrosion resistance in the acidic waste containing nitric acid. Corrosion of stainless steels in nitric acid medium is made more severe due to accumulation of oxidizing corrosion products in the stored fluid over a long storage period. This calls for stainless steels that are not only resistant to sensitization but also have a low general corrosion rate. One of the forms of corrosion specific to nitric acid medium is the intergranular corrosion (IGC) due to the presence of inclusions. Therefore, stainless steels for use with nitric acid medium should have low levels of inclusions, be resistant to sensitization and IGC, and have low general corrosion rates. Control of sensitization in stainless steels has been traditionally done by (1) solution annealing, (2) stabilizing carbon with titanium or niobium, or (3) using low carbon grades. Each technique has its own limitations. A fourth approach[3,4,5] has been brought in recently. Control of the character of grain boundaries so as to have a high degree of randomization[3,4] has been shown to control sensitization, IGC, and intergranular stress corrosion cracking (IGSCC) in stainless steels.

Vitrification[2] of nuclear waste requires mixing of acidic solutions of high level waste with borosilicate slurry at a high temperature, leading to evaporation and finally fixation in the glassy matrix. The vitrification (process) pots made of alloy 690 (UNS N06690) have shown a limited operation life. The mechanism of the reaction between the molten glass and alloy 690 at operating temperatures of 950 °C to 1000 °C needs to be examined. The reactions between the materials of vitrification pots and the molten glass constituents have been examined.

The disposition of nuclear waste in underground repositories requires materials that can resist localized corrosion (pitting and crevice corrosion) at temperatures above 100 °C. It

V. KAIN and P. SENGUPTA, Scientific Officers, and P.K. DE, Head, Materials Science Division, and S. BANERJEE, Director, are with the Bhabha Atomic Research Centre, Mumbai 400 085, India. Contact e-mail: vivkain@apsara.barc.ernet.in

This article is based on a presentation made in the symposium "Effect of Processing on Materials Properties for Nuclear Waste Disposition," November 10–11, 2003, at the TMS Fall meeting in Chicago, Illinois, under the joint auspices of the TMS Corrosion and Environmental Effects and Nuclear Materials Committees.

also requires resistance against stress corrosion cracking in the ground waters. The following alloys, type 316 (UNS S31600) nuclear grade stainless steel, titanium grade 7 (UNS R52400), and alloy 22 (UNS N06022), have been selected[6] for underground disposal of spent nuclear fuels. Considerable amount of work on corrosion properties, welding, and phase transformations has been reported on alloy 22. It has been reported[7,8,9] that transformation to μ, P, and σ phases is possible especially during welding of alloy 22. Alternate alloys need to be explored that would be resistant to such transformations. Alloy 33 (UNS R20033) is reported[10] to have excellent corrosion properties even in acidic medium including nitric acid. The corrosion properties in a chloride containing environment have been evaluated in this study at an elevated temperature and compared with those of alloy 22.

This article describes the main approaches in controlling corrosion of stainless alloys in nuclear waste disposal applications. Section II deals with control of corrosion in a nitric acid medium. It describes the results of our studies on the mechanism of IGC in nonsensitized stainless steels due to the presence of inclusions. The development of nitric acid grade (NAG) stainless steels and the basis for its development are described. In Section III, the results on grain boundary modification to control sensitization are described. In Section IV, the failure modes of vitrification pots are enumerated and results on the reaction mechanism between the molten glass and alloy 690 are given. In Section V, results of the study on localized corrosion of an alternate material for underground disposal of nuclear waste, alloy 33 have been compared with those of alloy 22. Each of these aspects has been dealt with separately in Sections II through V, where recent experimental findings are reported and discussed.

II. CONTROLLING CORROSION IN NITRIC ACID MEDIUM

In the nitric acid medium, nitrate ions, in addition to hydrogen ions, act as oxidizing agents. The corrosion potential in nitric acid medium is in the transition regions of potentials from passive to transpassive, as shown in Figure 1. There are three main approaches that have to be employed to control corrosion in oxidizing nitric acid medium.

A. *Control of IGC*

The control of IGC in austenitic stainless steel is invariably sought to be achieved by reducing carbon levels. However, there is a limitation in reducing the carbon contents, because at carbon levels below ~0.015 wt pct, boron (that is commonly present in stainless steels as an impurity, at levels around 30 ppm) starts to precipitate out as chromium boride and leads to chromium depletion at grain boundaries.[11] In addition, carbon is a strong austenite former; therefore, one cannot independently reduce the carbon to very low levels without affecting austenite stability, which is required during fabrication of components. The solubility of carbon in the austenitic matrix is reduced if the nickel content is increased. However, nickel cannot be reduced to such low levels because it affects the austenite stability. Therefore, the approach adopted[12,13,14] for the type 304 L (UNS S30403) NAG grade of stainless steels is to keep carbon levels below 0.025 wt pct (preferably around 0.015 to 0.020 wt pct) and also to maintain nickel content between 10 and 11 wt pct. This ensures that for a stainless steel with chromium content between 18 and 20 wt pct, the precipitation of chromium carbides is at a minimum during welding. Thus, one can ensure that there would not be any continuous chromium depletion regions along a grain boundary that could have made the material prone to IGC. In order to further ensure that no grains would be covered with chromium depletion regions, the grain size of the NAG grade has been kept small (ASTM number 6-8). This increases the area of the grain boundaries over which chromium carbides precipitate.

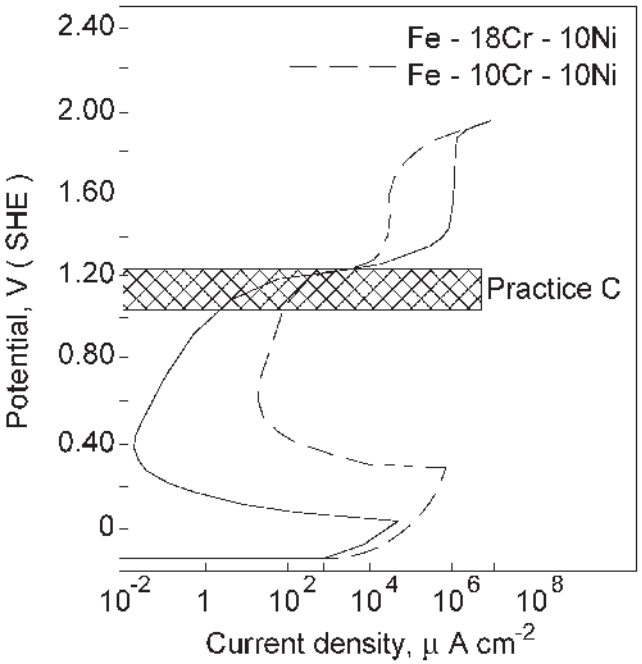

Fig. 1—The high operating potentials moving in the transpassive potential range as the concentration of oxidizing corrosion products increases during practice C ASTM, indicated in the polarization curve for type 304 stainless steel by the hatched region.

In oxidizing environments, the second method by which IGC can occur is by segregation[15,16,17] of silicon and phosphorus at grain boundaries. This would cause IGC only in highly oxidizing environments, *e.g.*, $HNO_3 + Cr^{+6}$ boiling solutions. In plants handling concentrated nitric acids at high temperatures, accumulation of corrosion products of stainless steels occurs. This makes the solutions highly oxidizing, leading to IGC due to segregation of elements at grain boundaries. The control of this form of corrosion is done by limiting the levels of silicon to 0.40 wt pct and of phosphorus to 0.035 wt pct. Further reducing silicon to 0.10 pct ensures freedom from IGC due to segregation of silicon at grain boundaries. The IGC of stainless steels without controlled levels of silicon and phosphorus takes place at corrosion potentials at transition from passive to transpassive potentials. Typical chemical composition of types 304L NAG and 310L NAG are shown in Table I along with the chemical composition of commercial purity stainless steels.

B. *Control of Manufacturing Related Corrosion*

The resistance to IGC of three different heats of type 304L stainless steels was tested. The chemical compositions of the

three heats are given in Table II. Samples from these heats were sensitized at 675 °C for 1 hour. The microstructures of the three heats of tubes developed after sensitization and electroetching in oxalic acid of the cross-sectional faces, per A262 ASTM, are shown in Figure 2. The sensitized samples from the three heats were exposed to practice C A262 ASTM for five periods of 48 hours each. The test solution was changed after each period. The corrosion rates of the heats after five periods of exposure in practice C are shown in Table II. It is seen from the table that two heats, A and B, had showed very high corrosion rates though the carbon content was low. The third heat, heat C, showed a lower corrosion rate of 0.533 mm/y (21 mpy), though its carbon level was higher at 0.028 pct. This is due to the presence of inclusions in heats A and B, as seen

Table I. Typical Chemical Composition of the NAG Stainless Steels (Weight Percent)

Grade of SS	Cr	Ni	C	Si	Mn	S	P	Others
Commercial purity 304L	18 to 20	8 to 12	<0.03	<1.0	<2.0	<0.030	<0.045	—
304L NAG	18 to 20	10 to 11	<0.02	<0.40	<1.8	<0.010	<0.025	N < 0.07 O < 0.01
310L NAG	25	21	<0.02	<0.20	<0.80	<0.010	<0.020	—

Table II. Chemical Composition (Weight Percent) and Corrosion Rate in the Fifth Period of Practice C A 262 ASTM of the Three Heats of Type 304L Stainless Steels Used in This Study

Heat	C	Cr	Ni	Mn	Si	S	P	Corrosion Rate, mm/y (mpy)
A	0.017	19.46	9.32	1.47	0.47	0.025	0.032	3.607 (142)
B	0.024	19.10	10.17	1.35	0.43	0.025	0.033	6.629 (261)
C	0.028	18.90	10.25	1.34	0.45	0.025	0.035	0.533 (21)

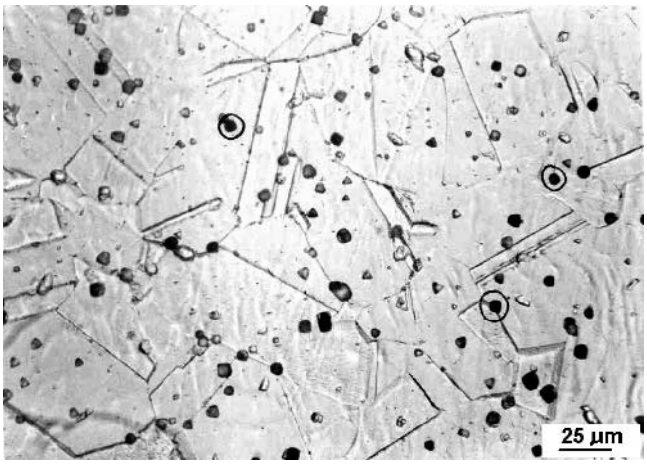

(*a*)

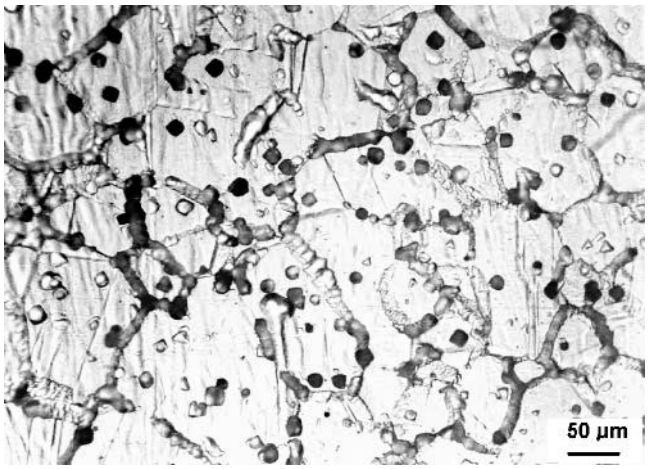

(*b*)

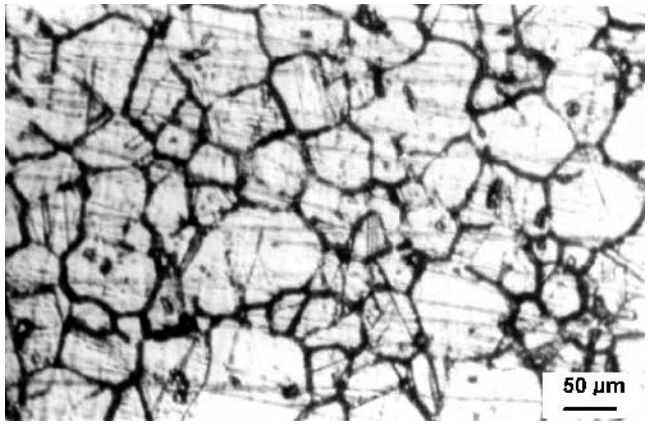

(*c*)

Fig. 2—Microstructure after sensitization heat treatment and oxalic acid etching showing (*a*) inclusions, a few shown by encircling, and step[26] structure for heat A; (*b*) dual[26] structure and inclusions for heat B; and (*c*) heavy dual structure for heat C of type 304 L stainless steels.

in Figure 2. Heat A showed a "step" microstructure (*i.e.*, no carbides/chromium depletion regions at the grain boundaries) but showed a high IGC rate of 3.607 mm/y (142 mpy). Heat B showed a "dual" structure (where chromium carbide precipitates/chromium depletion regions are present at the grain boundaries but do not completely encircle a grain) and heavy inclusions, and it resulted in a higher corrosion rate of 6.629 mm/y (261 mpy). Heat C, which did not have heavy inclusions, showed a moderate corrosion rate of 0.533 mm/y (21 mpy). This is consistent with the microstructure that is heavy dual. A microstructure showing at least one grain completely encircled by chromium depletion regions is termed a "ditch" structure. The longitudinal sections of the samples exposed to practice C A262 ASTM were examined under optical microscope after a light electroetching in oxalic acid for 20 seconds. The structure is shown in Figure 3(a). It can be seen that the attacked regions are wide at the end (exposed) faces and narrow along the longitudinal direction. This implies that the attack had started from the end faces. The attack had progressed along the direction of (a) the elongated inclusions and (b) the flow lines in the materials. These flow lines are clearly visible in Figures 3(a) and (b). Figure 3(b) shows that the attack had progressed along the grain boundaries only; even twin boundaries had undergone attack. The attack on twin boundaries, which remain unaffected even in sensitized stainless steels because these boundaries are resistant to sensitization, indicates that it is not dictated by sensitization. In order to check if the flow lines or the inclusions are responsible for the intergranular attack, electron probe microanalysis (EPMA) was done. A line scan starting from the matrix and running into the flow lines (marked in Figure 3(c)) was done for Fe, Cr, and Si. The X-ray line scans are shown in Figure 3(d). These indicate that there is a ~30 pct increase in chromium counts in the flow line regions. This segregation of chromium at the flow line regions has to be compensated by depletion of chromium at other regions. No measurement of chromium depletion/segregation of elements at grain boundaries could be done using EPMA, because this technique makes measurement from at least 1-μm depth. However, the mode of attack in practice C A262 ASTM was clearly intergranular (Figures 3(a) and (b)), which indicated that there was chromium depletion or segregation of Si or P at grain boundaries. This depletion of chromium was not less than 12 pct; otherwise, it could be detected by practice A A262 ASTM. The inclusions were identified to be rich in manganese, sulfur, and oxygen confirming that these are manganese (oxy) sulfide type of inclusions. Again,

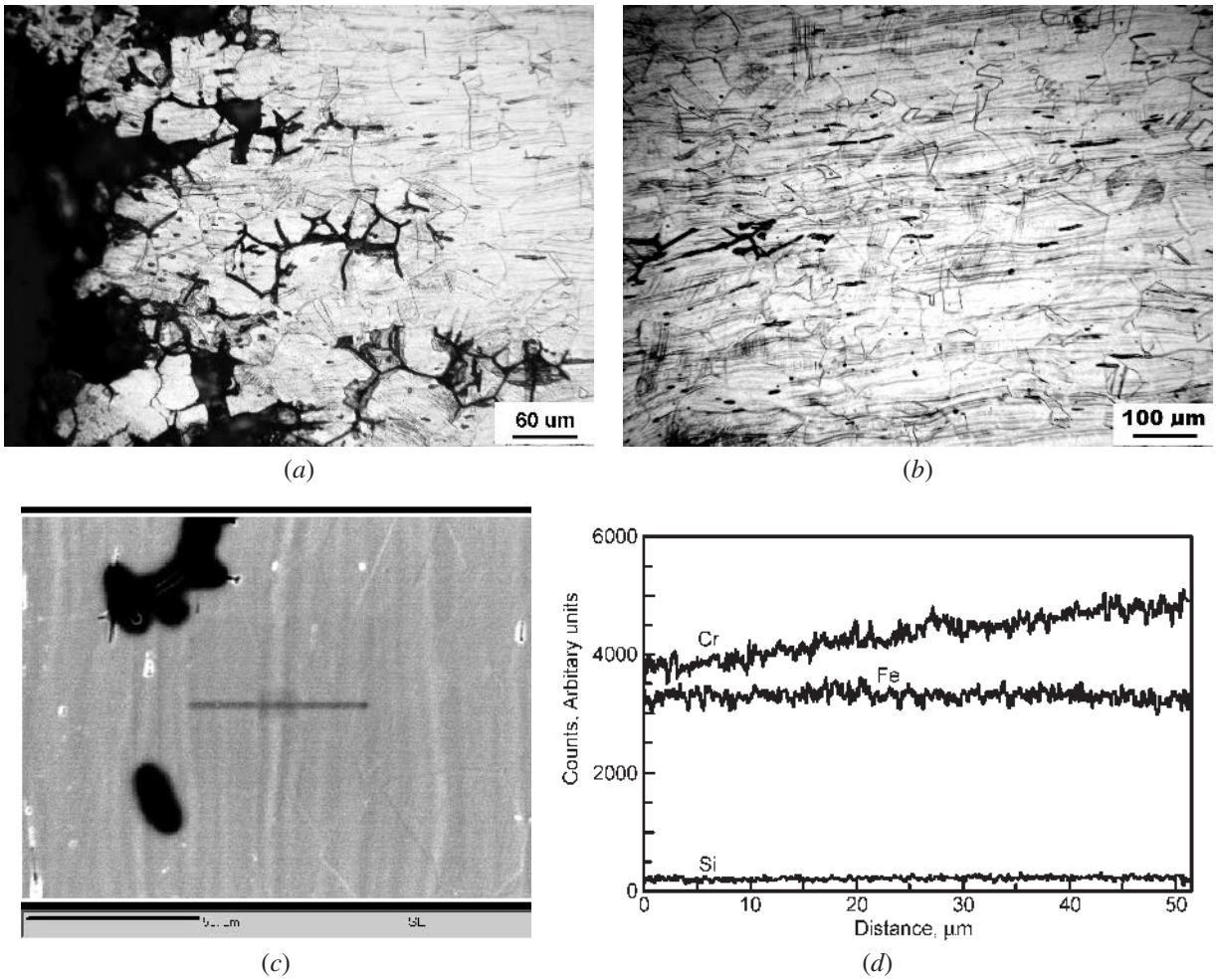

Fig. 3—The end grain corrosion attack is (*a*) the maximum at the end faces, showing grain dropping and progressing inward along grain boundaries, with twin boundaries also becoming corroded, and (*b*) intergranular and in the same direction as the alignment of stringer types of inclusions and flow lines in the material. (*c*) The flow lines in the material across which an X-ray scan is taken in EPMA that shows (*d*) ~30 pct enrichment of chromium in the flow line.

no depletion of chromium could be detected around these inclusions because the technique used (EPMA) is not sensitive to detect depletion on a nanometer scale. It has been reported recently[18] that sulfide inclusions have a thin layer of chromium depletion around them, and that is responsible for the pitting attack in stainless steels. However, this finding has not been confirmed by other studies[19,20] and remains to be proven. This clearly shows that type 304L stainless steels that contained inclusions but also showed heavy flow lines were prone to accelerated intergranular attack in practice C A262 ASTM. This study shows segregation of chromium along the flow lines. Stainless steels showing heavy flow lines and segregation of chromium along them are therefore prone to accelerated intergranular attack. Inclusions were much smaller in size compared to the depth of attack (Figures 3(a) and (b)). Such intergranular attack occurred even when there were no carbides/chromium depletion regions associated with precipitates in stainless steels, as in heat A. The presence of such carbides/chromium depletion regions around it enhanced the rate of attack, as seen for heat B. Flow lines form due to processing of stainless steels. Either improper hot working or heavy cold working, together with an insufficient solution annealing treatment, results in materials containing flow lines and segregation along them. These segregations along flow lines have to be removed by proper heat treatments.

Inclusions leading to severe corrosion attack in type 304L stainless steels were shown[21] to be mainly sulfides (and oxy sulfides) of manganese and iron. The corrosion rates of sensitized stainless steels increased 20 to 30 times due to the presence of these inclusions. The solution annealed (nonsensitized) stainless steels containing these types of inclusions also underwent IGC. This was due to dissolution of stringer types of sulfide inclusions from the exposed end (cross-sectional) faces. This caused accumulation of Cr^{+6} ions in the cavities that formed due to dissolution of inclusions. This makes the environment within the dissolved inclusions even more aggressive, and the high-energy grain boundaries start corroding, leading to IGC. However, chromium depletion caused by segregation of chromium along flow lines also leads to such heavy attack. Therefore, initiation of corrosion is due to dissolution of inclusions, but the propagation is accelerated by manufacturing related flow lines and chromium segregation along it. This form of corrosion occurs specifically in a strongly oxidizing environment. Therefore, "end grain corrosion" is a form of corrosion, often observed in highly oxidizing nitric acid environments, and is a manufacturing related problem. This is minimized by specifying a total inclusion rating of less than 4.5 per ASTM and freedom from segregation due to processing for the NAG grade. Another method by which the manufacturing process leads to end grain corrosion in austenitic stainless steels is by preferential attack on the segregated elements along accumulated dislocations due to cold working. The dislocation banding taking place along the direction of working as a result of cold working leads to segregation of elements such as niobium in stabilized stainless steels and silicon and phosphorus in nonstabilized grades. This makes such regions more prone to corrosion in strong oxidizing environments, and the exposed end faces of tubular products become corroded.

Specifically, the sulfide type of inclusions, termed "active inclusions," has to be avoided. The control of inclusions in NAG grade stainless steels is done by controlling the levels of sulfur and oxygen. Low levels of sulfur and manganese ensure that the manganese sulfide type of inclusions does not form. Other types of inclusions are controlled by limiting the dissolved oxygen content in the stainless steel to less than 0.01 pct but preferably below 50 ppm. This requires a special type of melting practices, especially secondary refining practices. After vacuum arc melting or vacuum oxygen decarburization, either electroslag remelting (ESR) or refining by steam and oxygen and nitrogen gas injection, *e.g.*, in Creusot–Loire–Uddeholm, is used to obtain proper chemical composition and low levels of inclusions.[22] The ESR route is known to result in minimum inclusions among commonly used techniques to reduce inclusions.

C. *Control of General Corrosion*

The corrosion of stainless steels in strong oxidizing nitric acid medium occurs in the transpassive potentials (represented by the transpassive part of a polarization curve for stainless steel in nitric acid medium, as shown in Figure 1). Therefore, any species that tends to increase the oxidizing power of the medium also increases its corrosion rate. The oxidation of the surface film, Cr_2O_3, to form chromic acid in the solution itself makes the environment more oxidizing and aggressive. The chromium-depleted regions in stainless steels (at the grain boundaries adjacent to chromium carbides formed in the heat-affected zones as a result of welding) get readily attacked in these oxidizing solutions. This provides more oxidizing ions in the solution, and the aggressiveness (or the oxidizing power) of the solution increases as the concentration of oxidizing ions increases in the solution with time. Therefore, it is important that the general corrosion rate of the stainless steel should be as low as possible in order to release a minimum number of oxidizing ions into the process solution. This aspect is especially applicable to components in which nitric acid fluids are recycled (or not refreshed periodically) as the corrosion products (in this case oxidizing, higher valence ions of iron and chromium) continue to accumulate. This further increases the oxidizing power of the process fluid. The concern regarding minimizing general corrosion rates is not as important for stainless steels that are used in components where the process nitric acid solution is used in a once through stream.

The general corrosion rate of austenitic stainless steels can be minimized by formation of a surface oxide film that is richer in chromium. This is helped by a small amount of cold work retained in the material. Cold work helps in increasing the dislocation density in the material. The diffusion rate of chromium along the dislocations is much faster than that along the austenitic matrix.[23] This increases the supply of chromium to the surface to form a strong, chromium-rich oxide film that protects it from fast general corrosion. This concept is used in the NAG stainless steels to allow retention of a small amount (5 to 10 pct) of cold work. Whether orientation of grains also changes in this process and controls the general corrosion rate still remains to be shown.

III. CONTROLLING SENSITIZATION BY INCREASED FRACTION OF RANDOM GRAIN BOUNDARIES

The stainless steels for waste management applications must be free from sensitization, IGC, and IGSCC. Though

low carbon grades are typically used for these applications, control of the nature of grain boundaries has so far not been used to control sensitization in stainless steels. Precipitation of chromium carbides at grain boundaries is a strong function of the energy of grain boundaries. The energy of grain boundaries varies from 20 to 835 mJ/m^2 in type 304 stainless steel.[24] The lower the energy of the grain boundary, the more difficult it is for precipitation to take place.

In this study, a 10-mm-thick plate of type 304 stainless steel (chemical composition: C0.055, Cr18.78, Ni9.60, Mn0.80, Si0.30, P0.0025, and S0.0015, all in wt pct) was cold rolled to achieve 80 pct reduction in thickness. The rolled plate was solution annealed at 1050 °C for 1 hour and water quenched. This annealed sample was sensitized at 675 °C for 1 hour. The microstructures of the surfaces after oxalic acid etching of the (1) as-received, (2) as-received and sensitized, and (3) 80 pct cold-rolled, solution-annealed, and sensitized material are shown in Figure 4. The material after 80 pct cold rolling, solution annealing, and sensitization heat treatment produced a structure (Figure 4(c)) that is highly resistant to sensitization. The microstructure of thus processed and sensitized material matches that of the as-received or annealed material (Figure 4(a)), though the material is a high-carbon type 304 stainless steel. The as-received material after sensitization heat treatment showed a ditch structure, indicating a high degree of sensitization (DOS). The DOS was evaluated by the double loop–electrochemical polarization reactivation (DL-EPR) test[25] in 0.5 M H_2SO_4 + 0.01 M KSCN (deaerated) at room temperature. The potential was scanned from the open circuit potential (OCP) to + 300 mV (SCE) and then scanned back to the OCP at a scan rate of 100 mV/min. The ratio of the maximum current during the reactivation scan to that during the activation scan multiplied by 100 was taken as the DL-EPR value. The DL-EPR values[25] of 0.01 to 0.1 generally indicate step structure, 0.1 to 5 indicate dual structure, and >5 indicate ditch structure. The measured DL-EPR values are reported in Table III. This also confirmed that the 80 pct cold-rolled, solution-annealed, and sensitized material has a very low DOS. Compared to it, the as-received and sensitized material showed a high DOS. These values match the microstructures shown in Figure 4.

The reason for this improvement in DOS after thermomechanical treatment was reported in earlier studies.[3,4] Type 304 stainless steel (C0.059, Cr18.10, Ni8.05, Mn1.43, Si0.41, P0.035, S0.010, N0.052, all in wt pct) was cold rolled by 20 to 80 pct reduction in thickness. The rolled samples were solution annealed at 1050 °C for 1 hour and water quenched. A sensitization heat treatment was given at 575 °C for 1 hour. The DOS was evaluated by the DL-EPR test, as described previously. The susceptibility to IGC was evaluated by practice B A262 ASTM[26] by exposure to a boiling solution of H_2SO_4 + $Fe_2(SO4)_3$ for 120 hours and measuring the weight loss. The susceptibility to IGSCC was evaluated by exposure to a boiling solution of 25 pct NaCl (acidified to a pH of 1.5) per G 123 ASTM.[27] The exposed samples were in constant strain condition and examined periodically for the presence of cracks. The nature of grain boundaries was measured by electron backscattered diffraction (EBSD) using orientation imaging microscopy[28] (OIM) in a scanning electron microscope. Electron backscattered diffraction generates the Kikuchi patterns, on an incident area on the sample (typically 20 μm × 20 μm area). The EBSD software automatically locates the positions of individual Kikuchi bands, compares these to theoretical data about the relevant phase, and rapidly calculates the three-dimensional crystallographic orientation. The whole process

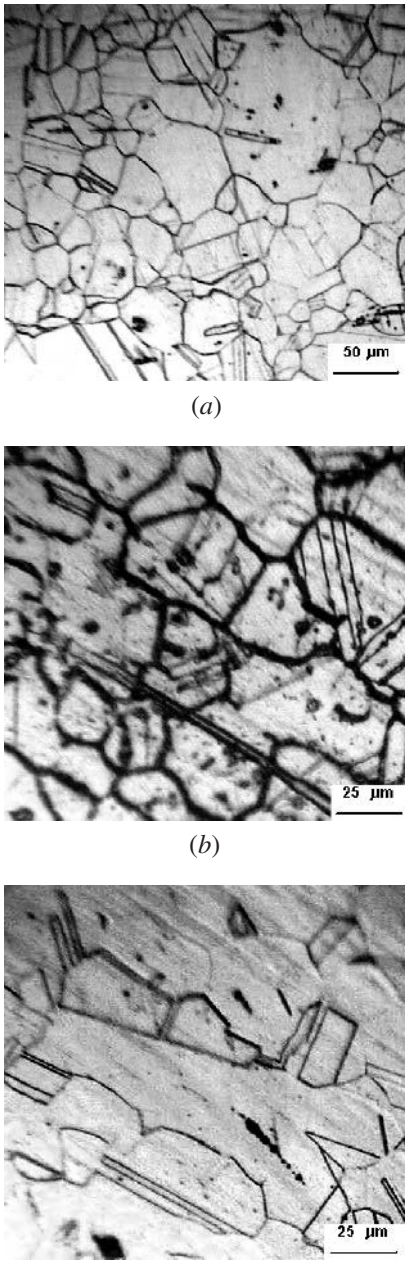

Fig. 4—Microstructures after oxalic acid etching showing (*a*) carbide-free structure for the as-received material, (*b*) heavily sensitized structure for the as-received and sensitized material, and (*c*) very few carbide precipitates in the 80 pct cold-rolled, solution-annealed, and sensitized material.

Table III. DL-EPR Values on Type 304 Stainless Steel

Material Condition	DL-EPR Value
As received (mill annealed)	0.005
As received + sensitized (675 °C 1 h)	2.73
80 pct cold rolled + solution annealed + sensitized	0.06

takes less than 0.05 seconds. In OIM,[28] the electron beam is stepped across the surface of the sample at regularly spaced points. The Kikuchi patterns are collected at each point, indexed by EBSD software, and the orientation information is stored. The OIM software assigns a specific Σ value to grain boundaries based on these measured orientations. The term Σ is the inverse of coincident sites.[24,28] The fractions of grain boundaries with different Σ values were measured, and fractions with $\Sigma = 3$ to 29 (special boundaries) and $\Sigma > 29$ (random boundaries) were derived.

The results from the DL-EPR test and the OIM are shown in Figure 5[4] for type 304 stainless steels after different degrees of cold rolling and solution annealing. It is clearly seen that the DOS increased as the degree of rolling increased from 20 to 60 pct reduction in thickness. At 80 pct reduction in thickness, there is a steep fall in DOS. This happened[3,4] when the fraction of random grain boundaries ($\Sigma > 29$) increased beyond 75 pct. Figure 6 shows the

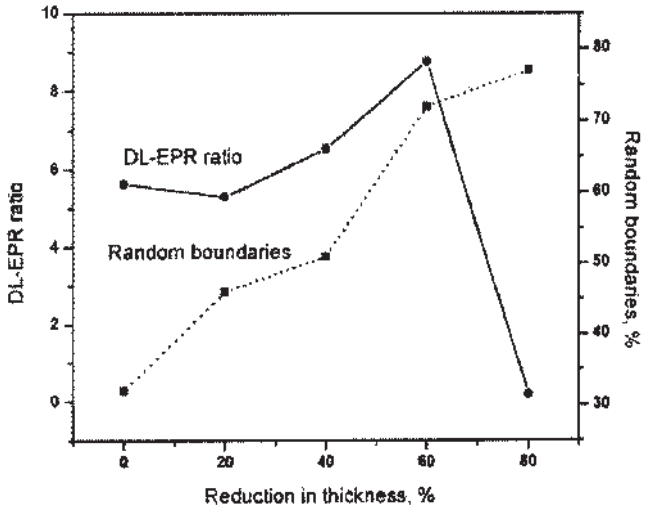

Fig. 5—The DL-EPR value and the fraction of random grain boundaries after different reduction in thickness by cold rolling, solution annealing, and sensitization heat treatment.[7]

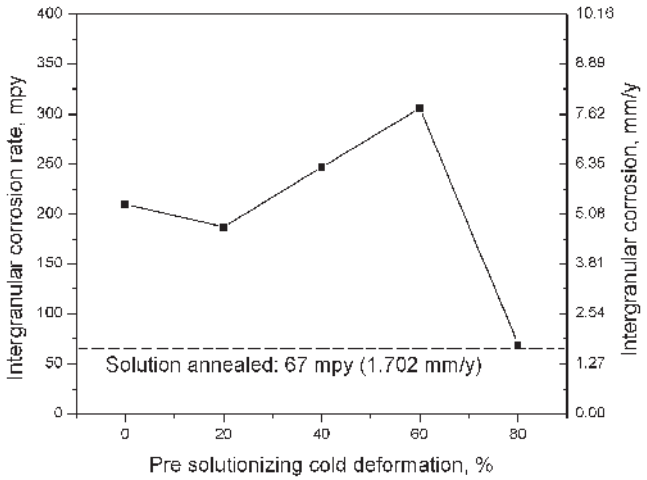

Fig. 6—The IGC rates after cold rolling, solution annealing, and sensitization, in mils per year (mpy), in the practice B A 262 ASTM. The values shown in brackets are the corrosion rates in mm/y.

corrosion rates on cold-rolled, solution-annealed, and sensitized samples in practice B A 262 ASTM. This shows a similar trend, where the IGC rate increased with the degree of rolling up to 60 pct reduction in thickness. At 80 pct reduction in thickness, the corrosion rate dropped sharply to levels comparable to that for the solution-annealed (nonsensitized) material. These were confirmed from microstructures developed after oxalic acid etching and those developed after the EPR test.

The IGSCC tests showed[4] a similar trend, with transgranular cracking observed in the annealed and no cracking for the 80 pct cold-rolled, solution-annealed, and sensitized samples in 144 hours of exposure to G 123 ASTM. The other materials, 20 to 60 pct cold-rolled, annealed, and sensitized, showed IGSCC in 144 hours of exposure. Typical cracks observed in different samples are shown in Figure 7.[4]

The results from OIM indicated that the fraction of random grain boundaries increased from 32 pct in the as-received material to 77 pct in the 80 pct cold-rolled and solution-annealed material. Only when the fraction of random grain boundaries increased beyond 75 pct was the beneficial effect in sensitization, IGC, and IGSCC observed. It has been shown by the bond percolation theory[29] that there is a continuous connectivity of

(*a*)

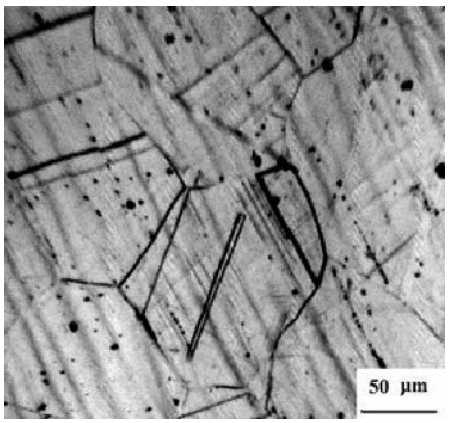

(*b*)

Fig. 7—The nature of cracks observed after 144 h exposure in 25 pct acidified solution of 25 pct NaCl showing (*a*) intergranular cracking[7] for the 40 pct cold-rolled annealed and sensitized material and (*b*) no cracks for the 80 pct cold-rolled, annealed, and sensitized type 304 stainless steel.

grain boundaries of a particular type (or sensitized boundaries) when the fraction of that type of boundary increases beyond 75 pct. At 75 pct of the boundaries, the random boundaries are continuously connected together by random boundaries. Hence, the beneficial effects of random boundaries would be seen only after 75 pct of the boundaries are random. Random boundaries are known to have a high diffusion rate of chromium. A continuously connected network of random boundaries would provide fast supply of chromium to the depleted regions that form as a result of precipitation of chromium carbides. This would quickly erase any depleted chromium regions. Thus, the bond percolation theory provides an explanation for the observed resistance to sensitization, IGC, and IGSCC for the materials with a high fraction of random boundaries.

The thermomechanical treatment thus provides a method to control sensitization, and susceptibility to IGC and to IGSCC, by controlling the nature of grain boundaries. In another reported study,[5] it was shown that a 5 pct reduction in thickness followed by a controlled annealing heat treatment increased the fraction of twin boundaries. This was shown[5,30] to result in improved resistance to sensitization and susceptibility to IGC. Twin boundaries are known to have lower energy; hence, the precipitation of chromium carbides is difficult.

IV. ALLOY 690—MOLTEN GLASS INTERACTIONS

Alloy 690 is used as the material for vitrification and susceptor pots for fixing the reprocessed nuclear waste in a glassy matrix. These pots have shown a limited operation lifetime. The main causes of failures are (1) temperature excursion due to operational problems and (2) corrosive conditions in the vitrification pots due to boric acid, concentrated nitrates, and sulfates.

To study the reaction between the molten glass and alloy 690, a tube of alloy 690 (chemical composition 27.75Cr, 8.5Fe, 0.30Mo, 0.011C, 0.10N, 0.18Mn, 0.13Si, 0.002S, 0.007P, and remaining Ni, all in wt pct) containing the borosilicate glass was annealed at 950 °C for 24 hours in air. The composition of the borosilicate glass was waste oxides 43.8, $SiO_2$34.1, $B_2O_3$6.4, Na_2O0.2, $TiO_2$6.2, and MnO9.3, all in wt pct. A cross section of the reacting surface of alloy 690 was examined by EPMA. Figure 8(a) is the backscattered electron image show-

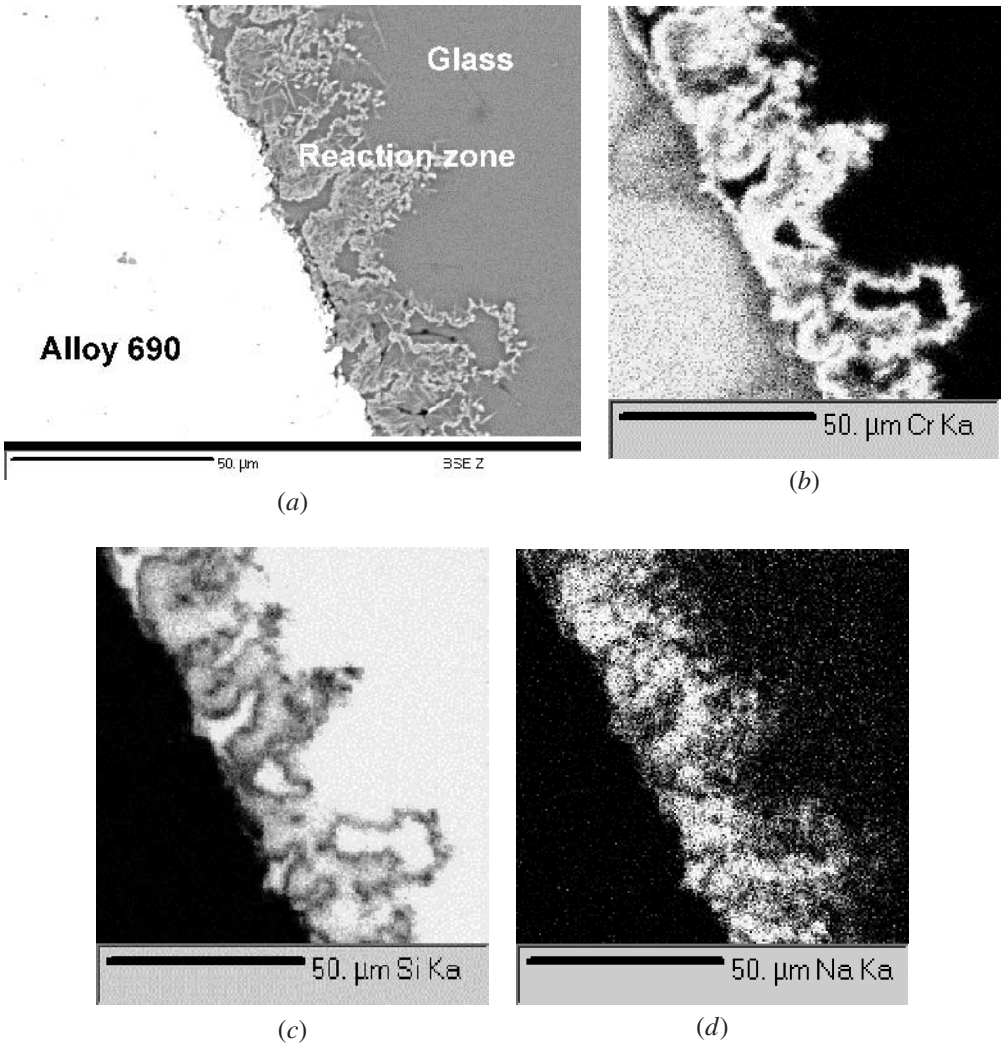

(*a*) (*b*) (*c*) (*d*)

Fig. 8—The reactions between the molten glass and alloy 690 in 24 h of exposure at 950 °C. (*a*) The backscattered image showing the reaction products at the interface. Elemental mapping showing (*b*) depletion of chromium in alloy 690 and formation of chromium-rich reaction products on the glass side of the interface that is also (*c*) depleted in silicon and (*d*) enriched in sodium.

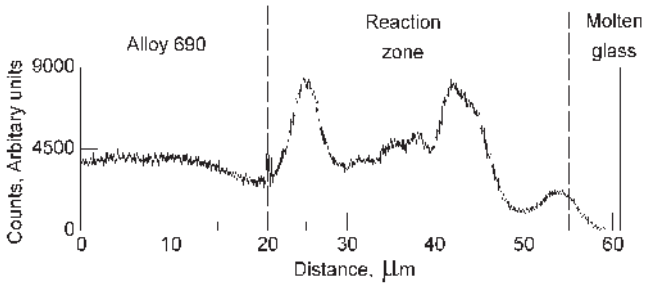

Fig. 9—X-ray scan showing depletion of chromium from the surface of alloy 690 after exposure to molten glass for 24 h at 950 °C. The chromium is enriched in the reaction zone.

ing development of a reaction zone between the molten glass and alloy 690. Figure 8(b) shows depletion of chromium on the alloy 690 surfaces near the reacting interface. A distance of 10 μm was found to be depleted. On the glass side, there was depletion of silicon near the reaction interface, enrichment of sodium, and also formation of chromium-rich phase at the interface. These are shown in Figures 8(b) through (d). The X-ray line scans were taken across the reaction interface, and the chromium K_α profile across the interface is shown in Figure 9. This shows depletion of chromium in alloy 690 near the interface and enrichment of chromium in the reaction zone on the glass side. A depth of 10 μm from the alloy surface is seen to be depleted of chromium and the chromium content on the alloy surface has reduced to half of its concentration in the alloy. The concentration of chromium in the reaction zone on the glass side is shown to have doubled from that present in the alloy.

A sample of alloy 690 was used with molten glass for 2 years at 950 °C to 1000 °C in intermittent operations. Analysis of this sample also showed chromium depletion from the alloy surface. The alloy 690 with depletion of chromium at the surface had become magnetic. This was confirmed by measurements with a ferrite meter, which showed FN numbers greater than 30. It has been shown that depletion of chromium in alloy 800[28] and in alloy 600[29] makes the materials magnetic, and measurements of magnetic susceptibility of these alloys have been correlated[31,32] to degree of sensitization and also to levels of chromium in the chromium depletion zones at grain boundaries. These results show that chromium is selectively removed from the surfaces of alloy 690 in contact with molten glass at 950 °C to 1000 °C. The loss of chromium on the surfaces is bound to change the surface properties and hence their corrosion rates at elevated temperature. The depletion of chromium from the surfaces of alloy 690 shown in this study provides an explanation for fast corrosion of alloy 690 in service with molten glass at elevated temperatures.

V. ALLOYS 33 AND 22 FOR UNDERGROUND REPOSITORY APPLICATIONS

The materials for underground repository applications have to resist localized corrosion at elevated temperatures. Alloy 22 has been shown[8,9] to resist localized corrosion up to 110 °C. The welded components of alloy 22 have been shown[6–9] to have μ and P phases that affect its resistance to localized corrosion. Alloy 33 is another material that has

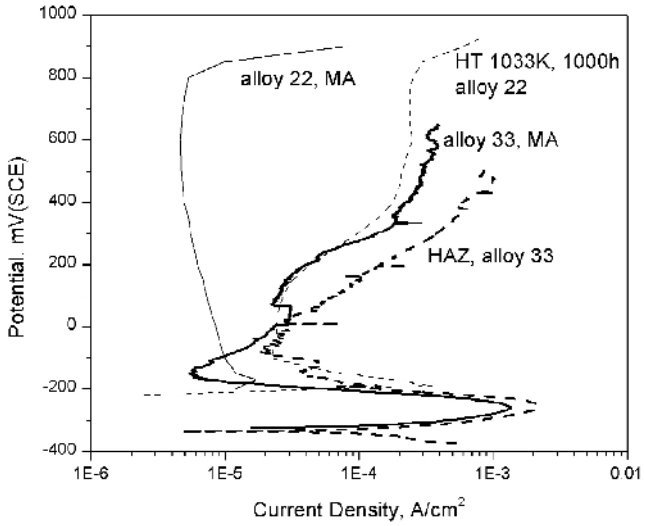

Fig. 10—Anodic polarization behavior of alloys 22 and 33 in 1 M HCl at 65 °C showing better passivation characteristics and resistance to localized corrosion of alloy 22.

excellent resistance to localized corrosion in hot chloride environments and also in nitric acid environments.[10] In this study, the electrochemical polarization behavior of welded alloy 33 (chemical composition: Cr32.75, Ni31.35, Mo1.49, Mn0.63, Si0.30, Cu0.54, C0.012, N0.40, S0.002, and P0.014, all in wt pct) is evaluated in 1 M HCl at 65 °C. Alloy 33 was welded by tungsten inert gas welding. The heat-affected zone and the base material parts of the weldment were separately exposed in the polarization experiments by masking all other parts. These polarization curves were compared with that[33] for alloy 22 in mill-annealed condition and after a heat treatment at 760 °C for 1000 hours under similar conditions. The comparative polarization curves obtained at a scan rate of 50 mV/min are shown in Figure 10.

It is seen from the figure that alloy 22, after long-term heat treatment, also shows lower current density than alloy 33 in its mill-annealed condition. Only alloy 22 in its mill-annealed condition retains passivity in the highly aggressive chloride environment at 65 °C. This indicates that alloy 33 is prone to pitting in an environment containing chloride ions at elevated temperatures even in its mill-annealed condition. However, alloy 22 retains passivity under similar conditions but tends to loose passivity when secondary phases form after long-term heat treatment. Such secondary phases (μ and P phases) are rich[7,9] in chromium and molybdenum and are associated with the depletion regions of these elements. Such phases are easily formed in welded structures.

It has been reported[33,34] that the regions depleted of molybdenum get attacked in reducing environments such as HCl and regions depleted of chromium get attacked in oxidizing environments such as nitric acid. Therefore, it is indicated from the results that phases rich in molybdenum formed during welding for alloy 33 that resulted in depletion of molybdenum around them. The identification of these phases in the welded sample of alloy 33 used in this study is yet to be done. Therefore, welded structures of alloys 33 and 22 are prone to form regions depleted of chromium and molybdenum, resulting in deterioration of localized corrosion

properties. The phase stability of these alloys needs to be increased. Alloy 22 is otherwise resistant[6,8,9] to localized corrosion in chloride ion bearing environments at elevated temperatures.

VI. CONCLUSIONS

The resistance to corrosion of austenitic alloys in waste management applications is a critical aspect that requires understanding of the basic mechanisms of corrosion, production of controlled purity alloys, and proper fabrication techniques to avoid secondary precipitates. The following conclusions emerge from this article.

1. Inclusions and segregation along flow lines induced IGC in the highly oxidizing nitric acid medium. Therefore, sulfide/oxysulfide types of inclusions and segregation along flow lines have to be minimized in stainless steels for applications involving highly oxidizing nitric acids.
2. The controlled chemical composition and controlled microstructure of type 304 stainless steel (termed NAG) resists sensitization and offers a low general corrosion rate in nitric acid medium. This allows the use of stainless steel in the nitric acid environment for long-term storage.
3. The resistance to sensitization of stainless steels increased by increasing the fraction of random grain boundaries. Once the fraction of random boundaries increased over 75 pct, the continuous connectivity of random boundaries provided resistance to sensitization, IGC, and IGSCC in hot chloride environments.
4. The material of construction of the vitrification pots, alloy 690, has been shown to react with the molten glass at 950 °C to 1000 °C and cause depletion of chromium at the surfaces of alloy 690. This affects surface film formation and corrosion resistance at elevated temperatures.
5. Both the mill-annealed and the heat-affected zone of welded alloy 33 have been shown to pit during anodic polarization experiments at 65 °C in HCl. Under similar conditions, the mill-annealed alloy 22 has been reported to retain good passivity, indicating a high resistance to pitting corrosion in chloride bearing environments.

ACKNOWLEDGMENTS

The authors thank Mr. K.N. Adhe, Materials Science Division, Bhabha Atomic Research Centre, for help in the electrochemical polarization experiments on alloy 33. The authors thank Mr. A. Laik, Materials Science Division, Bhabha Atomic Research Centre, for help with the EPMA of the stainless steel sample.

REFERENCES

1. "Shaping Third Stage of Indian Nuclear Programme," http://www.dae.gov.in/publ/3rdstage.pdf, 2003; and "Long Term Vision of the Department of Atomic Energy," http://www.dae.gov.in/publ/vision.pdf, 2003.
2. Kanwar Raj: *Proc. 14th Annual Conf. of Indian Nuclear Society and 1st BRNS Conf. on Nuclear Fuel Cycle*, Kalpakkam, Dec. 17–19, 2003, Baldev Raj and P.R. Vasudev Rao, eds., Indian Nuclear Society, Mumbai, 2003, pp. IT/1-18.
3. D. Wasnik, V. Kain, I. Samajdar, B. Verlinden, and P.K. De: *Acta Mater.*, 2002, vol. 50 (18), pp. 4587-4601.
4. D. Wasnik, V. Kain, I. Samajdar, B. Verlinden, and P.K. De: *ASM J. Mater. Eng. Performance*, 2003, vol. 12 (4), pp. 402-07.
5. M. Shimada, H. Kokawa, Z.J. Wang, Y.S. Sato, and I. Karibe: *Acta Mater.*, 2002, vol. 50, p. 2331.
6. G.M. Gordon: *Corrosion*, 2002, vol. 58 (10), pp. 811-25.
7. M.J. Cieslak, T.J. Headley, and A.D. Romig: *Metall. Trans. A*, 1986, vol. 17A, pp 1986-2035.
8. Larry Paul: *Waste Management Conf. 2001*, Tucson, AZ, Feb. 25–Mar. 1, 2001.
9. Raul B Rebak: *Effects of Metallurgical Variables on the Corrosion of High-Nickel Alloys*, ASM Handbook 13A, ASM INTERNATIONAL, Metals Park, OH, 2003, pp. 279-86.
10. VDM Report No. 26, VDM, Werdohl, Germany, 2002. http://www.kruppvdm.de_pdf/VDMReport26_c.pdf.
11. T. Gladman: *Mater. Performance*, 1989, vol. 28 (2), p. 699.
12. Vivekanand Kain, S.S. Shinde, and H.S. Gadiyar: *ASM J. Mater. Eng. Performance*, 1994, vol. 36 (6), pp. 699-705.
13. Vivekanand Kain and P.K. De: *Trans. Indian Inst. Met.*, 2003, vol. 56 (1), pp. 31-37.
14. Vivekanand Kain and P.K. De: *Proc. Conf. on Materials and Technologies for Nuclear Fuel Cycle—MRPI 2003*, Dec. 15–16, 2003, Baldev Raj, K. Bhanu Shankar Rao, P. Shankar, and N. Murali, eds., at Chennai by the Board of Research in Nuclear Science and Indian Nuclear Society, Kalpakkam, pp. 9-22.
15. A.J. Sedriks: *Corrosion Stainless Steels*, John Wiley & Sons, New York, NY, 1996, p. 110.
16. J.S. Armijo: *Corrosion*, 1968, vol. 24, p. 24.
17. H. Coriou, J. Hure, and G. Plante: *Electrochem. Acta*, 1961, vol. 5, p. 105.
18. M.P. Ryan, D.E. Williams, R.J. Chater, B.M. Hutton, and D.S. McPhail: *Nature*, 2002, vol. 415, p. 770.
19. Q. Meng, G.S. Frankel, H.O. Colijn, and S.H. Goss: *Corrosion*, 2004, vol. 60, p. 346.
20. M.P. Ryan and D.E. Williams: *Nature*, 2003, vol. 424, p. 390.
21. Vivekanand Kain, S.S. Chouthai, and H.S. Gadiyar: *Br. Corr. J.*, 1992, vol. 27 (1), pp. 59-65.
22. B.V. Patil, A.H. Cahn, and R.J. Choulet: *Steelmaking and Refining*, AISE Steel Foundation, Pittsburgh, PA, 1998, pp. 715-18.
23. Paul G. Shewmon: *Diffusion in Solids*, McGraw-Hill, New York, NY, 1963, p. 175.
24. L.E. Murr: *Interfacial Phenomenon in Metals and Alloys*, Addison-Wesley Publishing Company, Reading, MA, 1975; reprinted by *Teck Books*, Fairfax, VA, 1991.
25. A.P. Majidi and M.A. Streicher: *Corrosion*, 1984, vol. 40 (11), pp. 584-93.
26. ASTM A 262, *Annual Book of Standards*, ASTM, West Conshohocken, PA, 2000, vol. 3.01.
27. ASTM G 123: *Annual Book of Standards*, ASTM, West Conshohocken, PA, 2000, vol. 3.01.
28. *Electron Backscatter Diffraction in Materials Science*, Adam I. Schwartz, Mukul Kumar, and Brent L. Adams, eds., Kluwer Academic, New York, NY, 2000.
29. M.A. Gaudett and J.R. Scully: *J. Electrochem. Soc.*, 1993, vol. 140, pp. 3425-35.
30. H. Kokawa, M. Shimada, and Y.S. Sato: *JOM*, 2000, vol. 52 (7), pp. 34-37.
31. A. Borello and A. Mignone: *Br. Corr. J.*, 1982, vol. 17, pp. 176-83.
32. M. Kowaka, H. Nagano, T. Kudo, and Y. Okada: *Nucl. Technol.*, 1981, vol. 55, pp. 394-404.
33. R.B. Rebak, N.E. Koon, and P. Crook: in *Electrochemical Approaches to Selected Corrosion and Corrosion Control Studies*, P.L. Bonora and F. Daflorian, eds., IOM Communications, London, 2000, pp. 245-54.
34. R.B. Leonard: *Corrosion*, 1969, vol. 25, p. 222.